On the speciation of iodine in aerosol

Juan Carlos Gómez Martín[1*], Alfonso Saiz-Lopez[2], Carlos A. Cuevas[2], Alex R. Baker[3], Rafael P. Fernández[4].

[1] *Instituto de Astrofísica de Andalucía, CSIC, 18008, Granada, Spain*

[2] *Department of Atmospheric Chemistry and Climate, Institute of Physical Chemistry Rocasolano, CSIC, Serrano 119, 28006 Madrid, Spain*

[3] *Centre for Ocean and Atmospheric Science, School of Environmental Sciences, University of East Anglia, Norwich, UK*

[4] *Institute for Interdisciplinary Science, National Research Council (ICB-CONICET), FCEN-UNCuyo, Mendoza, 5501, Argentina*

**Correspondence to:* Juan Carlos Gómez Martín (jcgomez@iaa.es)

Abstract

We have compiled and analyzed a comprehensive dataset of field observations of iodine speciation in marine aerosol. The soluble iodine content of fine aerosol (PM_1) is dominated by soluble organic iodine (SOI) (~50%) and iodide (~30%), while the coarse fraction is dominated by iodate (~50%), with non-negligible amounts of iodide (~20%). The SOI fraction shows an equatorial maximum and minima coinciding with the ocean 'deserts', which suggests a link between soluble iodine speciation in aerosol and ocean productivity. Among the mayor aerosol ions, organic anions and non-sea-salt sulfate show positive correlations with SOI in PM_1. Alkaline cations are positively correlated to iodate and negatively correlated with SOI and iodide in coarse aerosol. These relationships suggest that under acidic conditions iodate is reduced to HOI, which reacts with organic matter to form SOI, a possible source of iodide. In less acidic sea-salt or dust-rich coarse aerosols, HOI oxidation to iodate and reaction with organic matter likely compete.

1. Introduction

Iodine has a profound impact on tropospheric chemistry through its role in ozone depletion, particle formation and impact on the oxidative capacity (Saiz-Lopez et al., 2012). In a previous publication (Gómez Martín et al., 2021), we reported the spatial variability of total iodine (TI) in aerosol by compiling and homogenizing a comprehensive dataset of field observations at open ocean, insular and coastal locations, and appending to it previously unpublished measurements, spanning a period of 55 years. The analysis of the latitudinal and longitudinal dependence of TI in aerosol provided for the first time observational evidence from the field showing that the dominant global source of atmospheric iodine to the atmosphere is the reaction between iodide and ozone on the sea-water interface. After uptake on particle surfaces, iodine undergoes a rich aqueous-phase chemistry, which is known to depend on the origin and chemical properties of the aerosol (e.g. acidity (Baker & Yodle, 2021)) but still remains poorly understood. Iodine speciation determines whether recycling to the gas phase can

proceed through formation of volatile species, which is thought to occur via iodide (I^-), or aerosol becomes essentially an atmospheric iodine sink through accumulation of species assumed to be stable and unreactive, i.e. iodate (IO_3^-) (Vogt et al., 1999). However, current aerosol chemical schemes cannot explain the concentrations of I^-, IO_3^- and soluble organic iodine (SOI) observed in field campaigns. Models predict negligible concentrations of I^- following recycling to the gas phase and high concentrations of IO_3^-, while they not deal with SOI (Pechtl et al., 2007; Vogt et al., 1999). In contrast, many field observations report highly variable concentrations of I^-, IO_3^- and SOI in aerosol samples (see e.g. (Baker, 2004, 2005; Gäbler & Heumann, 1993; Lai et al., 2008; Wimschneider & Heumann, 1995)).

In this study we adopt the same strategy than in our previous work on total iodine to shed light on the processes that control the speciation of iodine in aerosol. We have compiled the available iodine speciation data from cruises and coastal and insular ground-based stations with the aim of inspecting the spatial variability of the ensemble and comparing them with other global ocean and aerosol variables. For completeness, we also analyze the size distribution of total and soluble iodine, which were not specifically addressed in our previous work (Gómez Martín et al., 2021). The questions that we want to address in this work are: Which species dominates the soluble iodine speciation at different latitudes and longitudes? Where is each species most abundant: in the fine or in the coarse fraction? Can we link the iodine speciation in fine and coarse marine aerosol to other atmospheric and oceanic variables? And is the iodine speciation correlated to the dominant chemical composition of the aerosol substrate?

2. Methods

2.1. Definitions

Aerosol iodine quantities are defined as in (Gómez Martín et al., 2021). Total iodine (TI) is given by the sum of total soluble iodine (TSI) and non-soluble iodine (NSI): TI = TSI + NSI. Total soluble iodine encompasses total inorganic iodine (TII = $[I^-]$ + $[IO_3^-]$) and SOI. Note that except for one recent organic speciation work (Yu et al., 2019), the only individual species reported in the majority of field measurement (Tables S1 and S2) are iodide (I^-) and iodate (IO_3^-). SOI is determined from the TSI, I^- and IO_3^- observations: SOI = TSI - $[I^-]$ - $[IO_3^-]$. The soluble speciation is the set of three ratios of the concentrations of I^-, IO_3^- and SOI to TSI.

Iodine in bulk aerosol and in the fine and coarse aerosol fractions are noted respectively as X_{bulk}, X_{fine}, X_{coarse} (X = TI, TSI). Particulate matter with diameter $d <$ x m is noted as PM_x, and TI and TSI for diameter $d <$ x m are noted as TI_x and TSI_x. Usually the cut-off between fine and coarse aerosol is stablished operationally at a particle diameter of 1 m. This reflects approximately the usual size classification of marine aerosol, characterized by the nuclei ($d < 0.1$ m), the accumulation mode (0.1 m $< d <$ 0.6 m) and the coarse mode ($d > 0.6$ m) (Seinfeld & Pandis, 1998). PM_1 encompasses the

nuclei and the accumulation mode and is composed mostly of sulfate aerosol (low pH), while coarse marine aerosol consists of sea-salt aerosol produced by bubble bursting and wave breaking.

2.2. Description and treatment of datasets

In this work we keep the same campaign labels used in our previous publication on total iodine (Gómez Martín et al., 2021), for consistency. Tables S1 and S2 list respectively the 16 cruises (C#) and 12 coastal ground-based (S#) campaigns where aerosol iodine measurements have been carried out. Iodine speciation measurements are heterogeneous and do not always cover the same species or group of species. The data can be classified in five groups according to the iodine species reported and their size segregation in fine and coarse aerosol, as shown in Tables S1 and S2, and summarized in Table 1. For some of the cruises where the size distribution of soluble iodine species was reported (C4, C6, C10, C14, C17, C19 and C20) there are also measurements of major ions (MI) available (Allan et al., 2009; Baker et al., 2006, 2007; Droste et al., 2021; Martino et al., 2014; Powell et al., 2015), which are used in this work to investigate potential relationships with the iodine observations. MI observations include Na^+, NH_4^+, Mg^{2+}, Ca^{2+}, K^+, Cl^-, NO_3^-, SO_4^{2-}, oxalate ($C_2O_4^{-2}$), Br^- and methanesulfonate ($CH_3SO_3^-$), and derived quantities such as non-sea-salt (nss) K^+, Ca^{2+} and SO_4^{2-} as defined in (Baker & Yodle, 2021). Na^+ is the sea-salt tracer. The precursor of $C_2O_4^{-2}$, oxalic acid is emitted from fossil fuel combustion, biomass burning and biogenic activity, and it is also an oxidation product of both biogenic (isoprene) and of anthropogenic (e.g. cycloalkanes) emissions (Zhou et al., 2015). Combustion of fossil fuel and biomass are a source of NO_3^-, while NH_4^+ is linked to ammonia emissions from agriculture, although it also has background marine sources. The non-sea-salt ions are tracers of biomass burning, mineral dust and sulfur emissions (volcanic, biogenic or anthropogenic), respectively (Martino et al., 2014). $CH_3SO_3^-$ and nss_SO_4^- are oxidation products of marine biogenic DMS (Andreae et al., 1999), but can also be linked to biomass burning, and agricultural and urban emissions.

Table 1. Summary of available field observations of iodine speciation in aerosol

Observations	**Cruises/Stations** [a]	**Data points**
TI and TSI in bulk	C5, C7, C11, C12 [b], C13, S14, S34, S35	167
TI size distribution	C12 [b], S1, S2, S4, S9, S20, S28, S31	133
TSI and speciation size distribution	C4, C6, C10, C12 [b], C14, C17, C19, C20, part of S32	158
Speciation in fine fraction only	C8, C9, part of S32	74
Speciation in bulk only	C3, C5, C7, C13, C18, S14, S35	152

[a] The campaign labels are defined in Tables S1 and S2 and their geographical location is shown in Figure 1.

[b] Speciation measurements for campaign C12 are reported in this work for the

first time. The campaign is described in (Gómez Martín et al., 2021)

Some aspects of data treatment are discussed in the Supplementary Text ST1. Questions related to analytical methods employed to determine iodine speciation, and in particular to potential speciation changes resulting from the use of cellulose filters and ultrasonication due to the formation of oxidants (e.g. H_2O_2) (Kanthale et al., 2008; Yodle & Baker, 2019) are discussed in the Supplementary Text ST2.

The fraction of TI in aerosol with $d < 1$ µm and $d > 1$ µm has only been reported in one campaign (C12). Other campaigns where the fraction of iodine in fine and coarse aerosol was measured report cascade impactor size-segregated data in several size bins (S1, S2, S4, S9 and S31). These data can be binned together for $d < 1$ µm and $d > 1$ µm to get the estimates of the distribution of TI between the coarse and fine fraction. Regarding TSI, three campaigns considered a different cut-off radius ($d < 2.5$ µm in campaigns C8, C9 and part of S32) and only report the soluble speciation for $PM_{2.5}$.

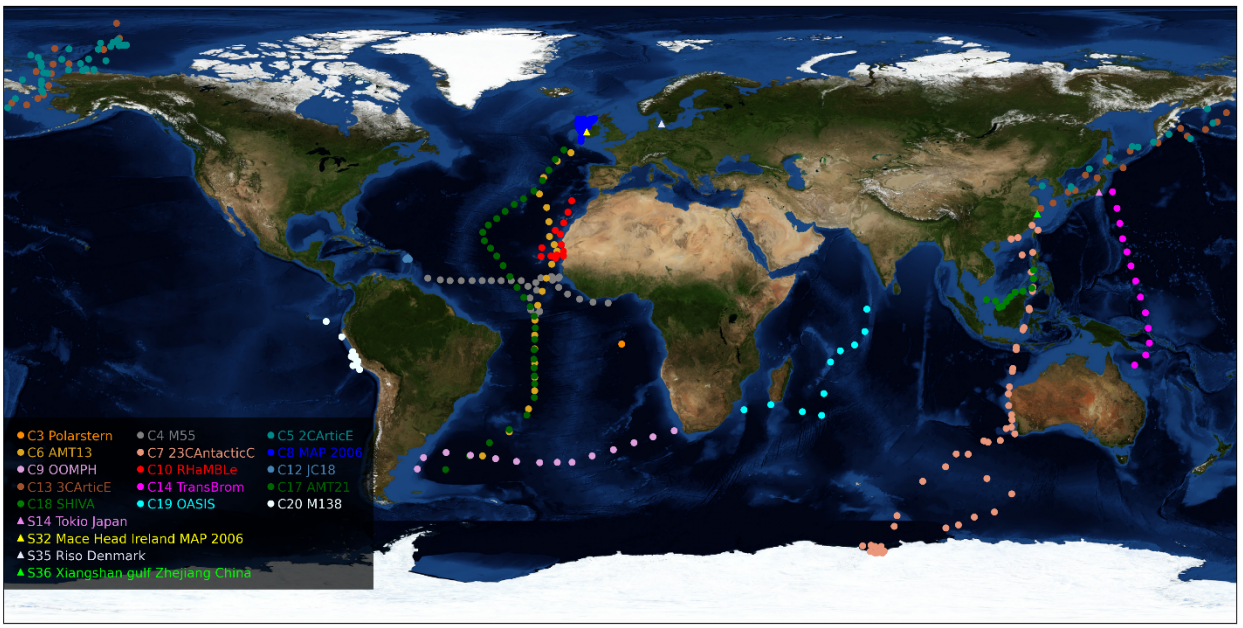

Figure 1. Geographical distribution of soluble iodine speciation observations (measurements of I^-, IO_3^- and SOI). Stations: triangles; Cruises: dots (see legend). For clarity, campaigns where only the TSI/TI fraction was measured are not included in the map.

Figure 1 shows the geographical distributions of the observations of iodine speciation in aerosol. Unfortunately, the speciation data is rather sparse, with an uneven spatial coverage, especially in the longitudinal coordinate. Most measurements were performed in the East and Central Atlantic and in the Eastern

Indian-Western Pacific region. Still, the campaigns sampled the complete range of latitudes, which enables a spatial analysis of the data. In contrast to total iodine measurements, long-term series of iodine speciation do not exist. Moreover, the published data are relatively recent, between 1983 and 2018, and most soluble speciation measurements were carried out between 2002 and 2014. This precludes a long-term trend analysis of the speciation data.

Field observations of TI, TSI, iodine enrichment in aerosol and soluble iodine speciation in aerosol in bulk, fine (PM1 or PM2.5) and coarse aerosol are compiled in the Supplementary Dataset S1. Field observations of major aerosol ions in fine (PM_1) and coarse aerosol are available in the Supplementary Dataset S2.

In order to investigate relationships between sea surface variables and the iodine speciation in aerosol, sea surface salinity (SSS), chromophoric dissolved organic mater (CDOM), detritus absorption at 443 nm and phytoplankton absorption at 443 nm composites have been obtained from the NASA online eard data open acces resounces. The SSS composite (25/08/2011 to 07/06/2015) was contructed with data from the Aquarius sattellite mission, while the Chl-a, CDOM, and 443 nm detritus and phytoplankton absorption composites (04/07/2002 to 20/05/2021) were constructed using MODIS-A satellite data.

3. Results and discussion

3.1. Size distribution of TI and TSI

About 40% of iodine (total and soluble) is contained in the PM_1 aerosol fraction. The content of TI and TSI in the $PM_{2.5}$ fine fraction is higher (~60%), as expected. The latitudinal and longitudinal dependences of the fraction of TI and TSI in fine aerosol for PM_1 and $PM_{2.5}$ are plotted in Figures S1 and S2, respectively. No clear spatial trends can be observed. The latitudinal plot suggests higher TI content in the fine aerosol towards the north pole.

3.2. Fraction of soluble iodine and distribution between coarse and fine aerosol

TSI/TI average, minimum and maximum ratios in bulk aerosol for different campaigns are listed in Table S3. Figure 2 shows TSI/TI statistics as a function of latitude for 10° zonal bins. These data were already used in our previous publication to scale TSI measurements to TI estimates (Gómez Martín et al., 2021), and therefore will be only briefly discussed. Concurrent TI and TSI observations are available from only eight campaigns (fist row in Table 1), while size segregated measurements of both TI and TSI are only available for campaign C12. In the bulk aerosol, an average of 65-80% of TI is in soluble form (Figure 2). The average TSI/TI ratio is 66%, while the TSI fraction derived from the slope of a TI vs TSI error-weighted fit is 79% (Gómez Martín et al., 2021). Seven TSI/TI ratios (four in C7 and three in C12) are larger than 1 beyond 2 analytical uncertainty and have been excluded from the soluble fraction statistical analysis, since TI = TSI + NSI TSI must be fulfilled.

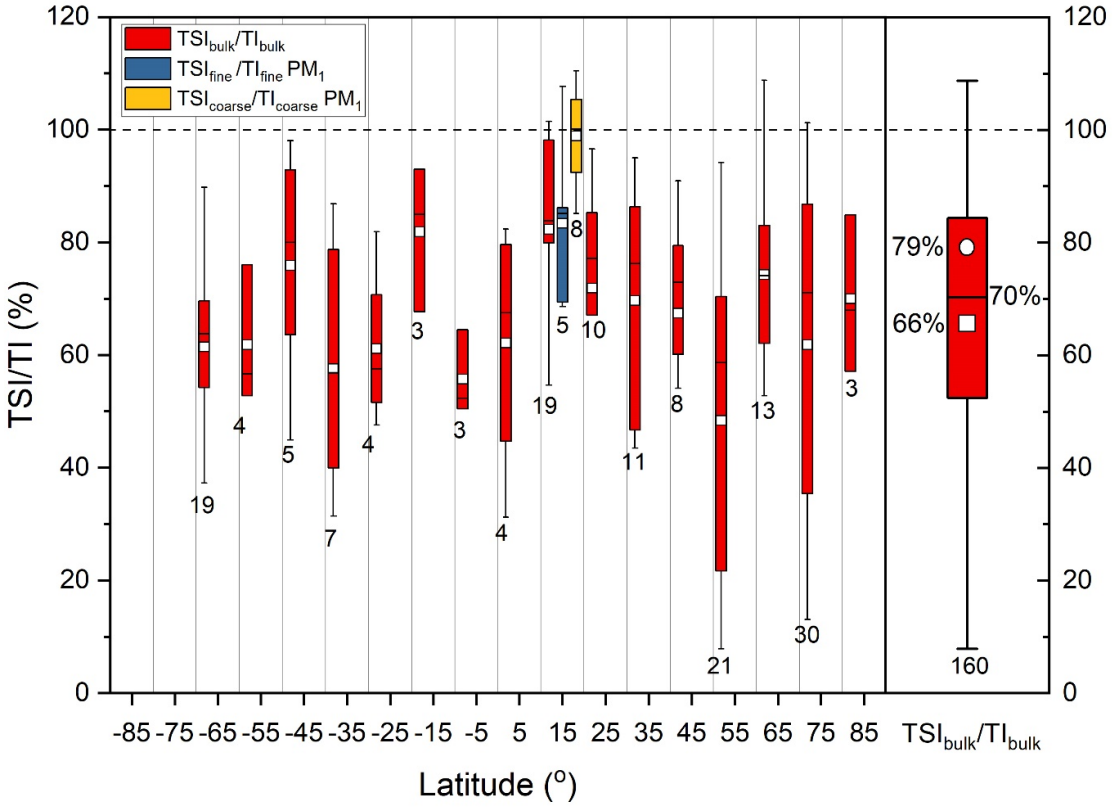

Figure 2. Left panel: latitudinal dependence of the TSI to TI ratio in bulk aerosol (red boxes), in the fine PM_1 fraction (blue) and the coarse fraction (yelow). Right panel: statistics of the TSI/TI ratio in bulk aerosol. The box and whiskers plot statistics are: interquartile range (box), 1.5 × interquartile range (whiskers), median (horizontal line), mean (square) and outliers (diamonds). The circle indicates the TSI fraction derived from the slope of the TI vs TSI error-weighted linear fit (Gómez Martín et al., 2021). The number of samples are indicated below the boxes.

Figure 2 does not show clear latitudinal trends in the bulk TSI/TI ratio. However, lower values were measured in some campaigns at high latitudes (C5, C7 and S35), and higher values in the tropical Atlantic (C12). Figure S3 shows TSI/TI in bulk aerosol as a function of longitude, for a zonal band between 55°S and 55°N. The campaigns in the Atlantic reporting both TI and TSI show TSI/TI ratios close to 90%-100%, while in the Eastern Indian - Western Pacific the ratio is closer to ~70%.

3.3. Soluble iodine speciation: iodide, iodate and SOI

Table S3 lists descriptive statistics of the bulk iodine speciation ratios measured in the field campaigns included in Table S1 and S2. Except for one station at high latitude (S35), the largest contribution to TI is TSI. It can be seen that the contributions of iodide, iodate and SOI to TSI are highly variable, and that in most cases the iodide fraction is non-zero.

Zonal averages in 10° latitude bins of the different X/TSI ratios (X = SOI, IO_3^-, I^-) are shown in Figure S4. There is an increase of SOI towards high latitudes (more pronounced in the southern hemisphere, SH), local SOI minima at tropical latitudes and a local SOI maximum at the equator. Iodide is enhanced towards high latitudes in the northern hemisphere (NH). Iodate is enhanced at tropical and equatorial latitudes in both hemispheres, with a possible local minimum at the equator. The global average contributions of SOI, iodate and iodide to soluble iodine in bulk aerosol are respectively 43%, 29% and 28% (Figure S4, right panel). Figure 3a shows 10° zonal averages as Figure S4 but using a 100% stacked column style, which allows better visualization of these trends. Iodide and SOI show opposite hemispheric gradients in bulk aerosol. Figures 3b and 3c show 100% stacked column plots for soluble iodine species in the fine (PM_1) and coarse fraction, respectively. Trends toward high latitudes cannot be seen in these plots because of the lack of size-segregated speciation measurements beyond 60°N and 50°S. The fine fraction (Figure 3b) is dominated by SOI, which shows a local maximum in the equatorial NH and local minima at 15°S-35°S and 25°N -40°N. I^- appears to anticorrelate to SOI, while IO_3^- is more or less constant, representing at most 20% of TSI. The coarse fraction (Figure 3c) is dominated by iodate (35% to 80%), except in the zonal band centered at 55°N, where almost all soluble iodine is SOI. Such high SOI fraction at this latitude is dominated by the MAP 2006 campaign at Mace Head and the Irish Sea (S32). The higher IO_3^- fraction in coarse aerosol with respect to PM_1 is at the expense of SOI (~20%) and to a lesser extent of iodide (~10%). SOI and IO_3^- appear anticorrelated in the coarse fraction, while I^- is approximately constant. The local maximum of SOI in the equatorial NH persists in coarse aerosol, concurrent in this case with an IO_3^- minimum.

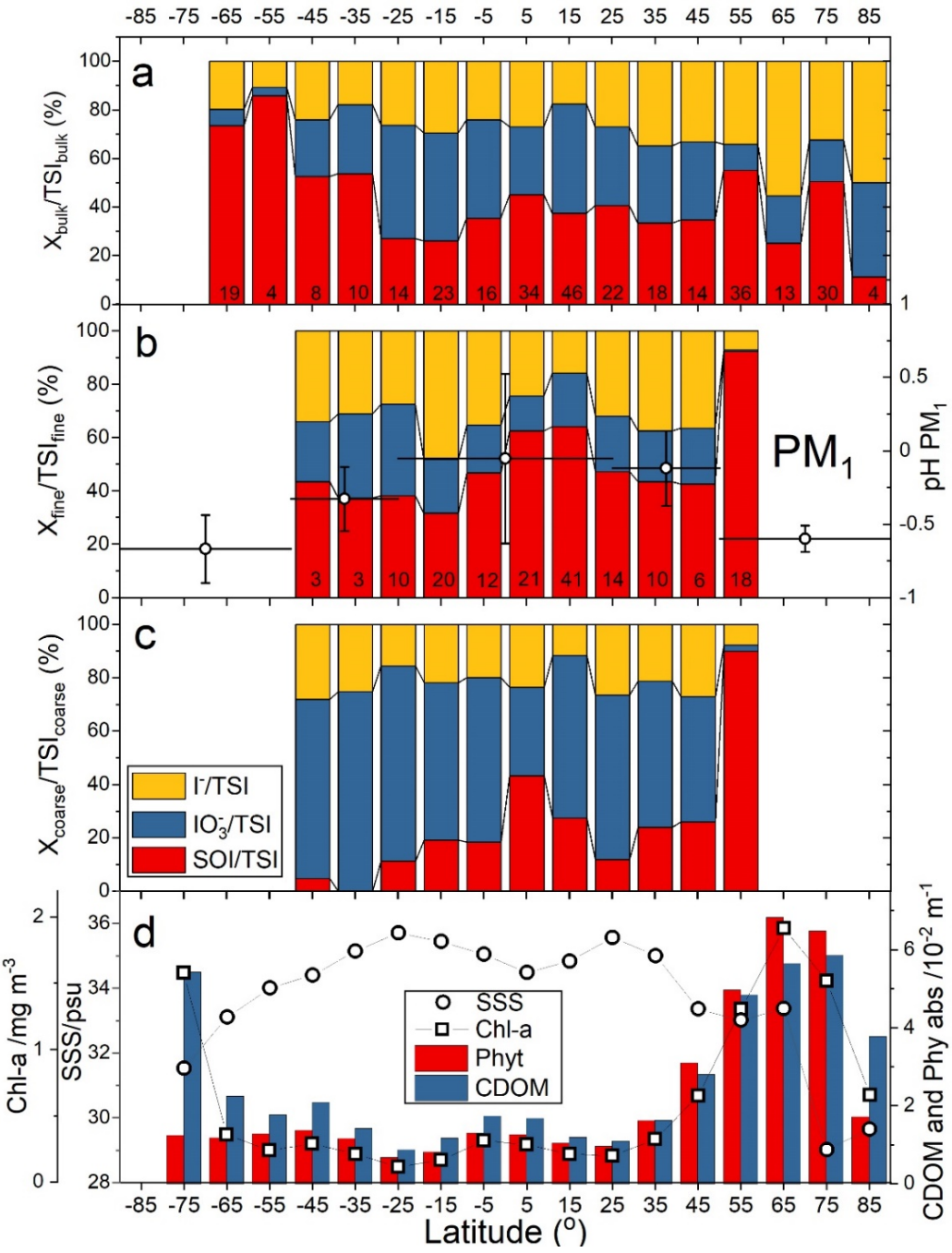

Figure 3. Latitudinal dependence of the TSI speciation. Panel a: in bulk aerosol; Panel b: in PM_1. Panel c: in coarse aerosol. Red, blue and yellow

stacked columns correspond to SOI, IO_3^-, I^-, respectively. Columns indicate data averages. The number of samples are indicated at the bottom of the columns. The latitudinal averages of PM_1 pH measured in the ATtom 1 and 2 campaigns is also plotted in panel b (averages: circles, meridional zones: horizontal lines, spread of measurements: error bars). Panel d: Sea surface salinity (SSS, circles) from the Aquarius sattellite mission, and Chlorophyll-a concentration (Chl-a, squares), CDOM and detritus absorption at 443 nm (CDOM, blue columns) and Phytoplankton absorption at 443 nm (Phyt, red columns) from the MODIS-A satellite mission. The satellite averages exclude data for land-locked seas where no measurements of iodine speciation exists (Baltic, Mediterranean, Caspian, Black, Red Seas and Persian Gulf).

The longitudinal variations of the X/TSI ratios (zonal band 55°S-55°N) are plotted in Figure S5. The iodide fraction appears to be enhanced in the Pacific, while the iodate fraction is higher at the Atlantic and Indian oceans. SOI shows a minimum in the eastern Atlantic and western Indian Ocean, which corresponds with regions of lower ocean productivity. For the sake of simplicity, we have not included data for PM_2 in Figures 3 and S5 (campaigns C8, C9 and part of S32). Analogous latitudinal and longitudinal plots for PM_1 and $PM_{2.5}$ are shown in Figure S6. Campaigns C8 and S32 (North Atlantic) and C9 (Southern Atlantic) show an extremely high SOI fraction.

3.4 Correlation between iodine speciation and major ions.

Since SOI/TSI = 1 – TII/TSI = 1 - $[I^-]$/TSI - $[IO_3^-]$/TSI, the SOI fraction is anticorrelated, by definition, with the TII fraction, and is expected to be anticorrelated with at least one of the two components of TII. Figure 4 shows that the SOI fraction is anticorrelated to both the iodide and iodate fractions in PM_1, but only anticorrelated to iodate in the coarse fraction. The iodate and iodide fractions are anticorrelated both in fine and coarse aerosol, but the anticorrelation is weaker in fine aerosol.

Correlations between MI concentrations in aerosol and iodine speciation ratios have been investigated for the seven cruises (C4, C6, C10, C14, C17, C19 and C20) reporting both types of measurements. This includes a total number of 132 iodine speciation measurements, although in practice each correlation pair may have less data as a result of non-detectable levels of a particular MI species. In addition to investigating correlations for the complete dataset (labelled "All" in Figure 4), the data has been divided in two groups: coastal (labelled "Coast") and open ocean (labelled "Ocean"), based on the distance between the sampling point and the closest continental coast. The idea behind this is highlighting the effect of crustal elements on the iodine speciation. A more rigorous approach would require classification of air masses by origin using back trajectories, which has been done previously for specific cruises (Baker & Yodle, 2021; Yodle & Baker, 2019). The Spearman rank correlation coefficient is used instead of the Pearson correlation coefficient, because the relationship between X/TSI (X = iodide, iodate, SOI) and MI is nonlinear because of the nature of the X/TSI ratio (always <1), as exemplified in Figure 6 for coastal coarse aerosol. Although

the Pearson coefficient captures most of the existing correlations, the Spearman rank coefficient is a more robust diagnostic for non-linear dependences and non-normally distributed data. Figure 4 shows Spearman correlation coefficients significant at $p = 0.01$ level.

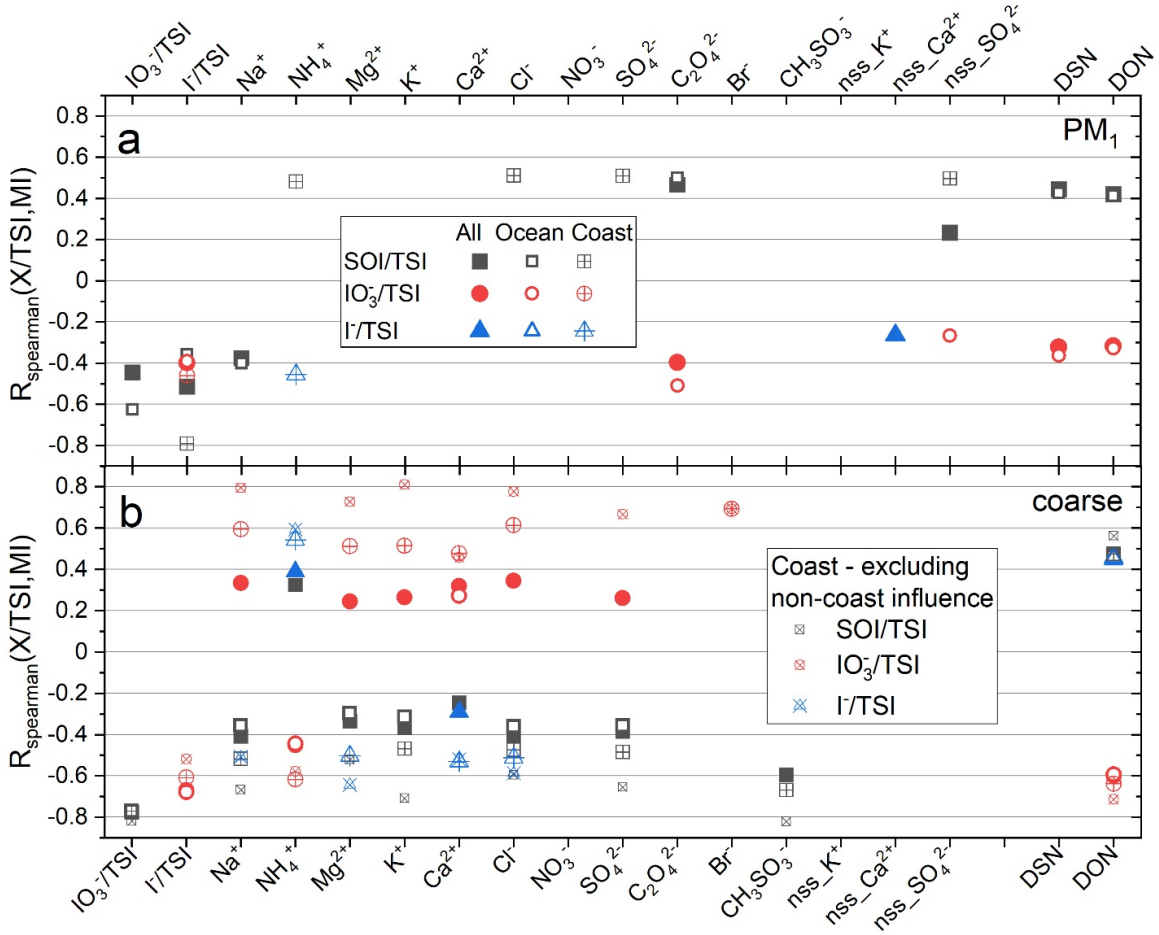

Figure 4. Spearman rank correlation coefficients between major ions in aerosol (MI), pH proxies (DSN and DON) and the soluble iodine speciation ratios X/TSI for campaigns C4, C6, C10, C14, C17, C19 and C20. Only correlations with p 0.010 are shown. Panel a: correlation coefficients for PM_1 aerosol. Panel b: correlation coefficients for coarse aerosol. Full, empty and crossed symbols correspond respectively to the complete dataset, open ocean data and coastal data. Panel b also contains a correlation re-analysis of the coarse coastal dataset excluding 5 datapoints of possible oceanic influence (small crossed symbols).

Iodine speciation variables and some MI may be causally linked, but they may also be correlated simply because existing correlations between the different

MI resulting from their common sources. Correlation-based hierarchical cluster analysis of the MI data (Supplementary Text S3) indicates five groups or clusters of variables in fine aerosol (Figure 5) that appear both in coastal (Figure S7) and open ocean data (Figure S8): the Na^+ group (sea-salt), the Cl^- group (Cl^- not linked to sea-salt in fine aerosol), the nss_SO_4^{2-} group (marine biogenic emissions), the nss_Ca^{2+} group (mineral dust) and the nss_K^+ group (biomass burning). NO_3, NH_4^+, $CH_3SO_3^-$ and $C_2O_4^{2-}$ appear associated to different groups in the coastal and open ocean subsets. In fine aerosol most of K^+, Ca^{2+} and SO_4^{2-} are non-sea salt ions, i.e. nss_X X, with X = K^+, Ca^{2+} or SO_4^{2-}. Five groups of variables can also be identified for coarse aerosol MI (Figures 5, S7 and S8): the sea-salt group (which includes tightly correlated Na^+, Cl^-, Mg^{2+} and K^+, as well as Br^- and SO_4^-), the mineral dust group (nss_Ca^{2+}), the NH_4^+ group, the $NO_3^-$and $C_2O_4^{2-}$ group (possibly fossil fuel combustion), and the biomass burning group (nss_K^+). For coarse aerosol Ca^{2+} it is also a non-sea salt ion (nss_ Ca^{2+} Ca^{2+}). The concentration of sea-salt- and dust-related ions is much higher in coarse aerosol (1-2 orders of magnitude).

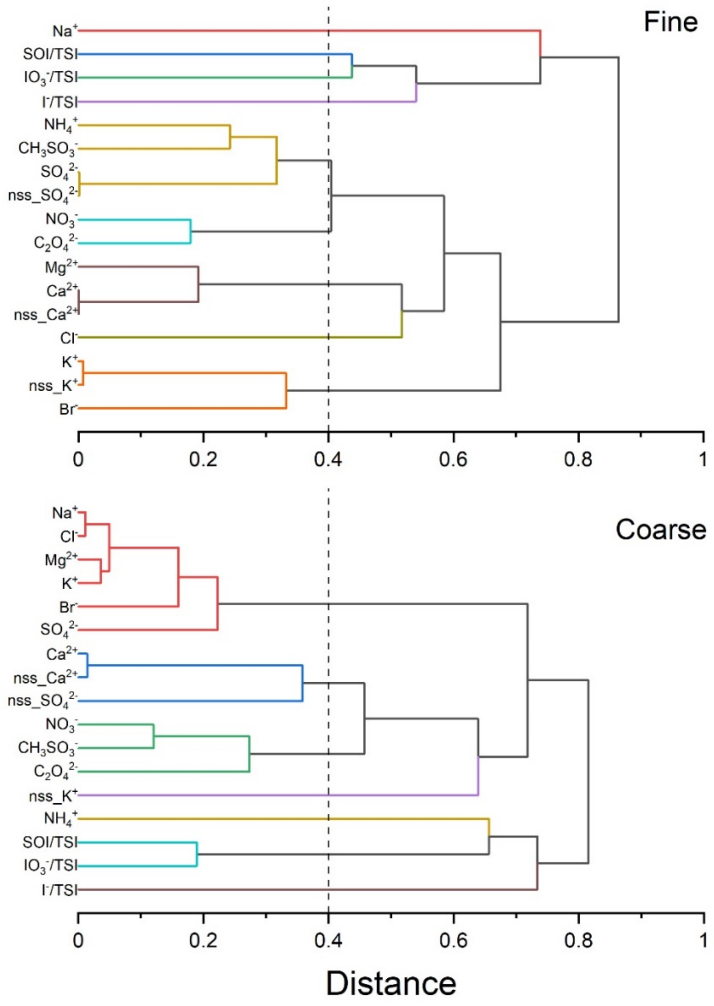

Figure 5. Absolute correlation hierarchical clustering dendrograms for iodine speciation and major ion (MI) variables. Top panel: fine (PM_1) aerosol. Bottom panel: coarse aerosol. The vertical dashed line indicates the distance ($R > 0.4$) chosen for the definition of clusters, which are identified by different colors.

In fine aerosol, the SOI fraction is positively correlated to some ions within the marine emissions cluster, as well as to Cl^- and $C_2O_4^{2-}$, for the coastal data subset. For the open ocean data subset, the SOI fraction is anticorrelated to Na^+, and positively correlated to $C_2O_4^{2-}$, while the IO_3^- fraction is also significantly anticorrelated to $C_2O_4^{2-}$. Note that $C_2O_4^{2-}$ ions are associated to different clusters in the two subsets (Figure S7-S8), although both are linked to biomass burning and agricultural emissions (the nitrogen-containing ions cluster for coastal fine aerosol and the nss_K^+ cluster in the open ocean).

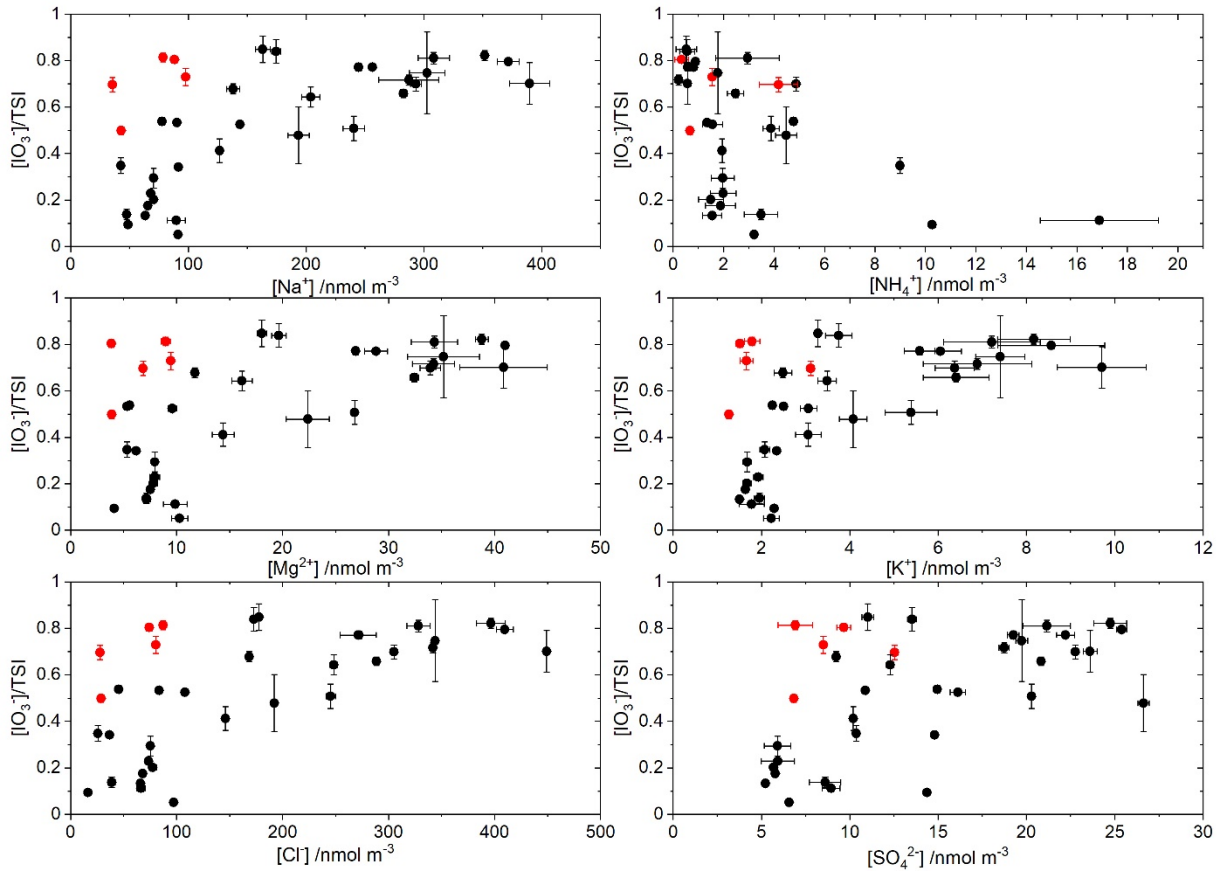

Figure 6. Scatter plots of iodate fraction versus selected MI species for coastal coarse aerosol. The red squares indicate a group of measurements off the Peruvian (n=3), the East American (n=1) and West African coast (n=1) that appear to deviate from the general trend, possibly because they are not under coastal but under open ocean conditions.

The strongest and more consistent correlations between the iodine speciation variables and MI are for coarse aerosol with the ions classified in the sea-salt, dust and the NH_4^+ cluster, and the correlations are stronger for the coastal data. The SOI and I^- fractions are anticorrelated to the ions of the Na^+ and Ca^{2+} clusters, while the IO_3^- fraction is positively correlated to the same ions. Conversely, the SOI and I^- fractions are positively correlated to NH_4^+ and the IO_3^- fraction is anticorrelated to NH_4^+, with the caveat that NH_4^+ concentrations are generally very low in coarse aerosol (Figure 6). Removing a few points of C20 (3 points off the West South-American coast, latitude < -15° and longitude < -76°) and of C4 (1 point off the East South American coast, latitude = 11° and longitude = -59°, and 1 point off the West African coast, latitude = 11° and longitude = -17°) enhances these correlations (Figure 4b), which is likely

a consequence of those data points being under open ocean rather than coastal conditions (Droste et al., 2021). Classification of data by air mass using back trajectory calculations may give higher correlations between iodide species and MI than with the simple coastal/open ocean classification used here (Baker & Yodle, 2021).

Proxies of pH based on aerosol MI observations are based on the cation-anion equivalent ratio or the ion balance method (Pye et al., 2020). In both methods, H^+ is assumed to balance the excess of anions. Two common versions of the cation-anion equivalent ratio are the degree of sulfate neutralization (DSN), the degree of neutralization (DON). None of these approaches are universal indicators of acidity, since they ignore gas-particle partitioning (Hennigan et al., 2015; Pye et al., 2020). The equivalent ratio in its different flavors may be able to distinguish alkaline particles from acidic particles reliably, although it is unable to quantify aerosol acidity (Hennigan et al., 2015). Figure 4 shows consistent anticorrelation between DON and iodate. Iodide is positively correlated to DON in coarse aerosol.

4. Discussion.

On average, 40% of aerosol iodine (total and soluble) exists in PM_1 and about 60% in $PM_{2.5}$. These percentages are consistent along both geographical coordinates. There is some evidence of higher concentration of iodine in fine aerosol at high latitudes, but only from campaign S28 (Barrie et al., 1994). The fraction of TSI in TI is also consistent across latitude and longitude (~65-80%). There is only one campaign at low latitudes (C12, (Gómez Martín et al., 2021)), reporting almost all TI being soluble, while another campaign (S35, (Zhang et al., 2016)) reports an extremely high non-soluble fraction (82%), with complete absence of iodate and SOI. Insoluble aerosol iodine does not seem to be linked to coastal new particle formation as previously speculated (Baker, 2004), since it appears to exist ubiquitously, and iodine driven new particle formations leads to iodic acid particles (Gómez Martín et al., 2020) and ultimately to iodate. The campaign reporting dominant non-soluble iodine took place in a coastal location, but not in open-ocean waters, and with some influence of continental air (Risø, Denmark, S35). Recent work has demonstrated the presence of abundant non-soluble iodine compounds in a continental location related to anthropogenic activities (Shi et al., 2021).

Iodine in enriched in aerosol compared to seawater, as a result of the uptake of gas-phase iodine compounds (Duce et al., 1983). As schematically depicted in Figure 7, the uptake of HI, HOI, $IONO_2$ leads to the formation of I^-, while uptake of iodine oxides is expected to form IO_3^-. Part of SOI present in seawater may be incorporated into aerosol from bubble bursting (primary SOI), but the fine mode dominance of SOI suggests that a larger fraction forms after sorption of gas phase iodine into particles (secondary SOI). It has been previously suggested that dissolved organic matter (DOM) in aerosol reacts with HOI to form SOI (Baker, 2005). Photolysis of SOI can potentially form I^-, as has been observed for alkyl halides (Jones & Carpenter, 2005; Martino et al., 2005). Organic

compounds and iodide could also form adducts (i.e. SOI) as reported by (Yu et al., 2019), leading to SOI-iodide interconversion, although the use of long ultrasonication times and cellulose filters makes the organic speciation reported in that work somewhat uncertain (Yodle & Baker, 2019).

The higher fractions of SOI and I^- in fine aerosol (respectively ~50% and ~30% on average for the complete dataset), and higher fraction of iodate in coarse aerosol (~50%) but with non-negligible iodide (~20%) has been previously documented for individual cruise datasets (Baker, 2004, 2005; Baker & Yodle, 2021; Droste et al., 2021). Figure 3 indicates that SOI, both in coarse and fine aerosol, has an equatorial maximum, minima in the tropical 'desert ocean' region, and again enhanced values at middle-high latitudes. This latitudinal distribution is reminiscent of the average latitudinal profiles of chl-a, phytoplankton absorption at 443 nm and CDOM and detritus absorption at 443 nm measured by MODIS-A (see Figure 3d), suggesting that organic compounds derived from oceanic emissions or incorporated in bubble bursting may exert some control on the SOI and I^- fractions. Some MI tracers of biogenic emissions are correlated to the iodine speciation in PM_1, suggesting that SOI forms from reactions between organics that have condensed on sulfate aerosol, forming DOM, and an iodine-containing species (HOI or I^-). The SOI and IO_3^- fractions in PM_1 are respectively correlated and anticorrelated to oxalate, $C_2O_4^{-2}$. Oxalate grows towards the NH, as can be expected from its partly anthropogenic sources, but the latitudinal profile shows some evidence of a superposed biogenic oceanic source (local equatorial maximum and tropical minima, Figure S9c). However, SOI is also anticorrelated to the sea-salt tracer Na^+ (which itself tracks SSS), which may indicate that there is less organic matter incorporated into aerosol by bubble bursting in the high SSS ocean 'deserts'.

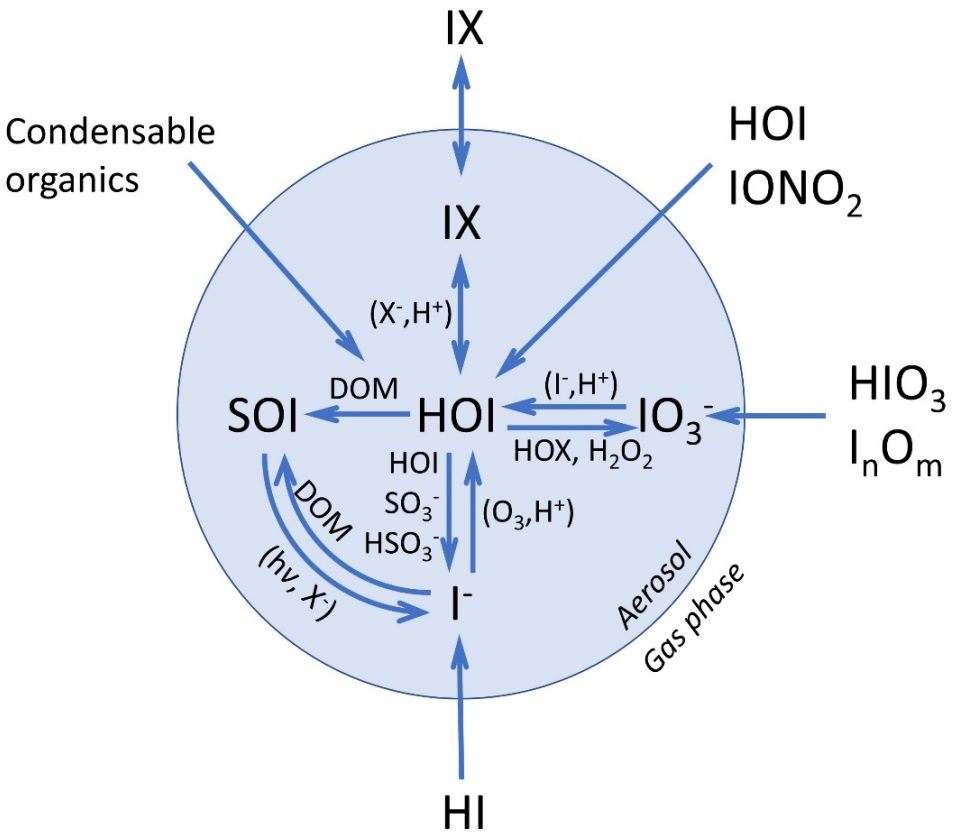

Figure 7. Chemical scheme of soluble iodine in aerosol adapted from Pechtl et al., 2007. The scheme includes SOI explicitly and highlights plausible routes between SOI, I^- and IO_3^- that may explain the variability observed in the global dataset of iodine speciation. Halogen atoms are noted in general as X (X = Cl, Br, I). I_nO_m (n = 2, m = 2,3,4) denotes iodine oxides. DOM refers to dissolved organic matter. Photolysis is indicated by hv.

The larger fraction of IO_3^- in coarse aerosol, with a non-negligible fraction of I^- (Figure 3), and the anticorrelation between the I^- and IO_3^- fractions both in fine and coarse aerosol (Figure 4), indicate that iodate is not a permanent iodine sink. The Dushman reaction and the Bray-Liebhafsky mechanism have been previously invoked to explain qualitatively the reduction of iodate to iodide under different acidity conditions (Koenig et al., 2020; Pechtl et al., 2007). I_2 formed from iodate reduction would be in equilibrium with HOI, which would react with DOM leading to the formation of SOI. Also, under acidic conditions, I^- could possibly be oxidized faster to HOI (Figure 7), explaining anticorrelation between SOI and I^- in PM_1, but not in coarse aerosol (Figure 4). Sulfate aerosol

is acidic (Pye et al., 2020), with pH generally between 1 and 3, that can also take negative values, as shown by the boundary layer pH data for PM_1 in Figure 3b (ATom campaigns (Nault et al., 2021)). Freshly emitted coarse sea-salt aerosol maintains its high pH for a very short period and then acidifies to values around 4-5 (Angle et al., 2021), and dust aerosol is basic in nature (Pye et al., 2020). The campaigns reporting iodine speciation and MI do not include concurrent measurements or estimates of pH. Observations of aerosol pH are only available for a limited number of field campaigns. Nevertheless, the correlations with MI species in Figure 4 are informative about potential links between acidity and the iodine speciation. The positive correlation between the iodate fraction and alkaline cations (coincident with a negative correlation for the SOI and iodide fractions) suggests a role of acidity in iodate reduction, since more alkaline ions would mean less acidic sea-salt or dust aerosol and accumulation of iodate (Baker & Yodle, 2021; Droste et al., 2021). Coarse aerosol collected close to the coast shows one order of magnitude higher content of crustal ions, which explains the enhanced correlations in Figure 4b. By contrast, Figure 4a shows a positive correlation in acidic PM_1 between SOI and nss_SO_4^{2-}. The pH proxies DSN and DON are anticorrelated to iodate and positively correlated to SOI, which supports the role of acidity in controlling the IO_3^- fraction. Hence, we suggest that the latitudinal variation of iodate and SOI in coarse aerosol (Figure S10) is mainly controlled by acidity, in contrast to fine aerosol, where the latitudinal variation of iodide and SOI appears to be controlled by organics (Figure S9).

5. Conclusions

There are some uncertainties regarding the different analytical methods employed in the determination of iodine speciation in aerosol (see supplementary text ST2 and (Yodle & Baker, 2019)), and we recommend that future work considers carefully the problems associated with the combination of cellulose filters and long time (and/or high power) ultrasonic extraction. However, the correspondence between the spatial trends of ocean productivity variables and the SOI fraction in marine aerosol determined from the global iodine speciation dataset compiled in this work, and the correlations between iodine speciation ratios and major ions concurrently measured in seven cruises indicate that the two acidity regimes and the availability of organics are major controlling factors of the iodide-iodate-SOI variability, as summarized in the chemical scheme in Figure 7. Future laboratory and modelling work needs to address the underlying chemical and photochemical reactions of this system, especially regarding the reactions between DOM and HOI and the photochemical processes linking SOI and iodide.

Data availability

MODIS-A Level 3 data products (chlorophyll-a, CDOM and detritus absorption at 443 nm and phytoplankton absorption at 443 nm) can be downloaded from NASA's Ocean Color Web (https://oceancolor.gsfc.nasa.gov/). SSS data from the Aquarius satellite mission can be downloaded from NASA's Physic Oceanography Distributed Active Archive Center (http://podaac.jpl.nasa.gov/SeaSurfaceSalinity/Aquarius).

Total iodine, total soluble iodine, iodine enrichment factors, iodine speciation and major ion aerosol observations in marine aerosol compiled for this work can be retrieved from doi:10.5281/zenodo.5588450.

Acknowledgements

The authors are grateful to Zhouqing Xie, Senchao Lai and Benjamin Gilfedder for assisting in the retrieval of historical data. J. C. G. M. acknowledges financial support from the State Agency for Research of the Spanish MCIU through the "Center of Excellence Severo Ochoa" award to the Instituto de Astrofísica de Andalucía (SEV-2017-0709) and the Ramon y Cajal Program (RYC-2016-19570). A.S.-L. acknowledges financial support from the European Research Council Executive Agency under the European Union's Horizon 2020 Research and Innovation programme (Project 'ERC-2016-COG 726349 CLIMAHAL').

References

Allan, J. D., Topping, D. O., Good, N., Irwin, M., Flynn, M., Williams, P. I., et al. (2009). Composition and properties of atmospheric particles in the eastern Atlantic and impacts on gas phase uptake rates. *Atmospheric Chemistry and Physics*, *9*(23), 9299–9314. https://doi.org/10.5194/acp-9-9299-2009Andreae, M. O., Elbert, W., Cai, Y., Andreae, T. W., & Gras, J. (1999). Non-sea-salt sulfate, methanesulfonate, and nitrate aerosol concentrations and size distributions at Cape Grim, Tasmania. *Journal of Geophysical Research: Atmospheres*, *104*(D17), 21695–21706. https://doi.org/https://doi.org/10.1029/1999JD900283Angle, K. J., Crocker, D. R., Simpson, R. M. C., Mayer, K. J., Garofalo, L. A., Moore, A. N., et al. (2021). Acidity across the interface from the ocean surface to sea spray aerosol. *Proceedings of the National Academy of Sciences of the United States of America*, *118*(2). https://doi.org/10.1073/pnas.2018397118Baker, A. R. (2004). Inorganic iodine speciation in tropical Atlantic aerosol. *Geophysical Research Letters*, *31*(23). https://doi.org/10.1029/2004gl020144Baker, A. R. (2005). Marine Aerosol Iodine Chemistry: The Importance of Soluble Organic Iodine. *Environmental Chemistry*, *2*(4), 295–298. https://doi.org/https://doi.org/10.1071/EN05070Baker, A. R., & Yodle, C. (2021). Indirect evidence for the controlling influence of acidity on the speciation of iodine in Atlantic aerosols. *Atmospheric Chemistry and Physics*, https://doi.org/10.5194/acp-2021-72.Baker, A. R., Thompson, D., Campos, M. L. A. M., Parry, S. J., & Jickells, T. D. (2000). Iodine concentration and availability in atmospheric aerosol. *Atmospheric Environment*, *34*(25), 4331–4336. https://doi.org/https://doi.org/10.1016/S1352-2310(00)00208-9Baker, A. R., Jickells, T. D., Biswas, K. F., Weston, K., & French, M. (2006). Nutrients in atmospheric aerosol particles along the Atlantic Meridional Transect. *Deep-Sea Research Part II: Topical Studies in Oceanography*, *53*(14–16), 1706–1719. https://doi.org/10.1016/j.dsr2.2006.05.012Baker, A. R., Weston, K., Kelly, S. D., Voss, M., Streu, P., & Cape, J. N. (2007). Dry and wet deposition of nutrients from the tropical Atlantic atmosphere: Links to primary productivity and nitrogen fixation. *Deep-Sea Research Part I: Oceanographic Research*

Papers, *54*(10), 1704–1720. https://doi.org/10.1016/j.dsr.2007.07.001Barrie, L. A., Staebler, R., Toom, D., Georgi, B., den Hartog, G., Landsberger, S., & Wu, D. (1994). Arctic aerosol size-segregated chemical observations in relation to ozone depletion during Polar Sunrise Experiment 1992. *Journal of Geophysical Research: Atmospheres*, *99*(D12), 25439–25451. https://doi.org/10.1029/94jd01514Droste, E. (2017). *Soluble Iodine Speciation in Indian Ocean Aerosols and its Impact on Marine Boundary Layer Chemistry (Master's Thesis)*. UEA and Wageningen UR. Retrieved from https://edepot.wur.nl/422789Droste, E., Baker, A. R., Yodle, C., Smith, A., & Ganzeveld, L. (2021). Soluble iodine speciation in marine aerosols across the Indian and Pacific Ocean basins. *Frontiers in Marine Science*, submitted.Duce, R. A., Winchester, J. W., & Van Nahl, T. W. (1965). Iodine, bromine, and chlorine in the Hawaiian marine atmosphere. *Journal of Geophysical Research*, *70*(8), 1775–1799. https://doi.org/10.1029/JZ070i008p01775Duce, R. A., Woodcock, A. H., & Moyers, J. L. (1967). Variation of ion ratios with size among particles in tropical oceanic air. *Tellus*, *19*(3), 369–379. https://doi.org/10.1111/j.2153-3490.1967.tb01492.xDuce, R. A., Arimoto, R., Ray, B. J., Unni, C. K., & Harder, P. J. (1983). Atmospheric trace elements at Enewetak Atoll: 1. Concentrations, sources, and temporal variability. *Journal of Geophysical Research, [Oceans]*, *88*(C9), 5321–5342. https://doi.org/10.1029/JC088iC09p05321Gäbler, H.-E., & Heumann, K. G. (1993). Determination of atmospheric iodine species using a system of specifically prepared filters and IDMS. *Fresenius' Journal of Analytical Chemistry*, *345*(1), 53–59. https://doi.org/10.1007/bf00323326Gilfedder, B. S., Lai, S. C., Petri, M., Biester, H., & Hoffmann, T. (2008). Iodine speciation in rain, snow and aerosols. *Atmos. Chem. Phys.*, *8*(20), 6069–6084. https://doi.org/10.5194/acp-8-6069-2008Gilfedder, B. S., Chance, R. J., Dettmann, U., Lai, S. C., & Baker, A. R. (2010). Determination of total and non-water soluble iodine in atmospheric aerosols by thermal extraction and spectrometric detection (TESI). *Analytical and Bioanalytical Chemistry*, *398*(1), 519–526. https://doi.org/10.1007/s00216-010-3923-1Gómez Martín, J. C., Lewis, T. R., Blitz, M. A., Plane, J. M. C., Kumar, M., Francisco, J. S., & Saiz-Lopez, A. (2020). A gas-to-particle conversion mechanism helps to explain atmospheric particle formation through clustering of iodine oxides. *Nature Communications*, *11*(1), 1–14. https://doi.org/10.1038/s41467-020-18252-8Gómez Martín, J. C., Saiz-Lopez, A., Cuevas, C. A., Fernandez, R. P., Gilfedder, B., Weller, R., et al. (2021). Spatial and Temporal Variability of Iodine in Aerosol. *Journal of Geophysical Research: Atmospheres*, *126*(9), e2020JD034410. https://doi.org/10.1029/2020JD034410Hennigan, C. J., Izumi, J., Sullivan, A. P., Weber, R. J., & Nenes, A. (2015). A critical evaluation of proxy methods used to estimate the acidity of atmospheric particles. *Atmospheric Chemistry and Physics*, *15*(5), 2775–2790. https://doi.org/10.5194/acp-15-2775-2015Jalkanen, L., & Manninen, P. (1996). Multivariate data analysis of aerosols collected on the Gulf of Finland. *Environmetrics*, *7*(1), 27–38. https://doi.org/10.1002/(sici)1099-095x(199601)7:1<27::aid-env159>3.0.co;2-3Jones, C. E., & Carpenter, L. J. (2005). Solar photolysis of CH2I2, CH2ICI,

and CH2IBr in water, saltwater, and seawater. *Environmental Science and Technology*, *39*(16), 6130–6137. https://doi.org/10.1021/es050563gKang, H., Xu, S., Yu, X., Li, B., Liu, W., Yang, H., & Xie, Z. (2015). Iodine speciation in aerosol particle samples collected over the sea between offshore China and the Arctic Ocean. *Advances in Polar Science*, *26*(3), 215–221. https://doi.org/10.13679/j.advps.2015.3.00215Kanthale, P., Ashokkumar, M., & Grieser, F. (2008). Sonoluminescence, sonochemistry (H2O2 yield) and bubble dynamics: Frequency and power effects. *Ultrasonics Sonochemistry*, *15*(2), 143–150. https://doi.org/10.1016/j.ultsonch.2007.03.003Koenig, T. K., Baidar, S., Campuzano-Jost, P., Cuevas, C. A., Dix, B., Fernandez, R. P., et al. (2020). Quantitative detection of iodine in the stratosphere. *Proceedings of the National Academy of Sciences*, *117*(4), 1860. https://doi.org/10.1073/pnas.1916828117Lai, S. C. (2008). *Iodine Speciation in Atmospheric Aerosols in the Marine Boundary Layer (Doctoral Dissertation)*. Johannes Gutenberg-Universität Mainz. Retrieved from http://doi.org/10.25358/openscience-3211Lai, S. C., Hoffmann, T., & Xie, Z. Q. (2008). Iodine speciation in marine aerosols along a 30,000 km round-trip cruise path from Shanghai, China to Prydz Bay, Antarctica. *Geophysical Research Letters*, *35*(21). https://doi.org/doi:10.1029/2008GL035492Lininger, R. L., Duce, R. A., Winchester, J. W., & Matson, W. R. (1966). Chlorine, bromine, iodine, and lead in aerosols from Cambridge, Massachusetts. *Journal of Geophysical Research*, *71*(10), 2457–2463. https://doi.org/10.1029/JZ071i010p02457Martino, M., Liss, P. S., & Plane, J. M. C. (2005). The photolysis of dihalomethanes in surface seawater. *Environmental Science and Technology*, *39*(18), 7097–7101. https://doi.org/10.1021/es048718sMartino, M., Hamilton, D., Baker, A. R., Jickells, T. D., Bromley, T., Nojiri, Y., et al. (2014). Western Pacific atmospheric nutrient deposition fluxes, their impact on surface ocean productivity. *Global Biogeochemical Cycles*, *28*(7), 712–728. https://doi.org/https://doi.org/10.1002/2013GB004794Nault, B. A., Campuzano-Jost, P., Day, D. A., Jo, D. S., Schroder, J. C., Allen, H. M., et al. (2021). Chemical transport models often underestimate inorganic aerosol acidity in remote regions of the atmosphere. *Communications Earth & Environment*, *2*(1), 93. https://doi.org/10.1038/s43247-021-00164-0Pechtl, S., Schmitz, G., & von Glasow, R. (2007). Modelling iodide – iodate speciation in atmospheric aerosol: Contributions of inorganic and organic iodine chemistry. *Atmos. Chem. Phys.*, *7*(5), 1381–1393. https://doi.org/10.5194/acp-7-1381-2007Powell, C. F., Baker, A. R., Jickells, T. D., W. Bange, H., Chance, R. J., & Yodle, C. (2015). Estimation of the atmospheric flux of nutrients and trace metals to the eastern tropical North Atlantic Ocean. *Journal of the Atmospheric Sciences*, *72*(10), 4029–4045. https://doi.org/10.1175/JAS-D-15-0011.1Pye, H. O. T., Nenes, A., Alexander, B., Ault, A. P., Barth, M. C., Clegg, S. L., et al. (2020, April 24). The acidity of atmospheric particles and clouds. *Atmospheric Chemistry and Physics*. Copernicus GmbH. https://doi.org/10.5194/acp-20-4809-2020Saiz-Lopez, A., Plane, J. M. C., Baker, A. R., Carpenter, L. J., von Glasow, R., Gómez Martín, J. C., et al. (2012). Atmospheric chemistry of iodine. *Chemical Reviews*, *112*(3). https://doi.org/10.1021/cr200029uSeinfeld,

J. H., & Pandis, S. N. (1998). *Atmospheric Chemistry and Physics*. New York: Wiley-Interscience.Sherwen, T. M., Evans, M. J., Spracklen, D. V, Carpenter, L. J., Chance, R., Baker, A. R., et al. (2016). Global modeling of tropospheric iodine aerosol. *Geophysical Research Letters*, *43*(18), 10012–10019. https://doi.org/10.1002/2016GL070062Shi, X., Qiu, X., Chen, Q., Chen, S., Hu, M., Rudich, Y., & Zhu, T. (2021). Organic Iodine Compounds in Fine Particulate Matter from a Continental Urban Region: Insights into Secondary Formation in the Atmosphere. *Environmental Science and Technology*, *55*(3), 1508–1514. https://doi.org/10.1021/acs.est.0c06703Tsukada, H., Hara, H., Iwashima, K., & Yamagata, N. (1987). The Iodine Content of Atmospheric Aerosols as Determined by the Use of a Fluoropore Filter® for Collection. *Bulletin of the Chemical Society of Japan*, *60*(9), 3195–3198. https://doi.org/10.1246/bcsj.60.3195Vogt, R., Sander, R., Von Glasow, R., & Crutzen, P. J. (1999). Iodine Chemistry and its Role in Halogen Activation and Ozone Loss in the Marine Boundary Layer: A Model Study. *Journal of Atmospheric Chemistry*, *32*(3), 375–395. https://doi.org/10.1023/a:1006179901037Wimschneider, A., & Heumann, K. G. (1995). Iodine speciation in size fractionated atmospheric particles by isotope dilution mass spectrometry. *Fresenius' Journal of Analytical Chemistry*, *353*(2), 191–196. https://doi.org/10.1007/bf00322957Xu, S., Xie, Z., Li, B., Liu, W., Sun, L., Kang, H., et al. (2010). Iodine speciation in marine aerosols along a 15000-km round-trip cruise path from Shanghai, China, to the Arctic Ocean. *Environmental Chemistry*, *7*(5), 406–412. https://doi.org/10.1071/en10048Yodle, C. (2015). *Iodine Speciation in Marine Aerosol (Doctoral Dissertation)*. UEA. Retrieved from https://ueaeprints.uea.ac.uk/id/eprint/56772Yodle, C., & Baker, A. R. (2019). Influence of collection substrate and extraction method on the speciation of soluble iodine in atmospheric aerosols. *Atmospheric Environment: X*, *1*, 100009. https://doi.org/10.1016/j.aeaoa.2019.100009Yu, H., Ren, L., Huang, X., Xie, M., He, J., & Xiao, H. (2019). Iodine speciation and size distribution in ambient aerosols at a coastal new particle formation hotspot in China. *Atmos. Chem. Phys.*, *19*(6), 4025–4039. https://doi.org/10.5194/acp-19-4025-2019Zhang, L., Hou, X., & Xu, S. (2016). Speciation of 127I and 129I in atmospheric aerosols at Risø, Denmark: insight into sources of iodine isotopes and their species transformations. *Atmos. Chem. Phys.*, *16*(4), 1971–1985. https://doi.org/10.5194/acp-16-1971-2016Zhou, Y., Huang, X. H., Bian, Q., Griffith, S. M., Louie, P. K. K., & Yu, J. Z. (2015). Sources and atmospheric processes impacting oxalate at a suburban coastal site in Hong Kong: Insights inferred from 1 year hourly measurements. *Journal of Geophysical Research: Atmospheres*, *120*(18), 9772–9788. https://doi.org/https://doi.org/10.1002/2015JD023531